Reaction Body Hydrodynamics for a Multi-DOF Point-Absorbing WEC

Timothy R. Mundon
Oscilla Power, Inc.
Seattle, WA, USA
E-mail: mundon@oscillapower.com

Brian J. Rosenberg
Oscilla Power, Inc.
Seattle, WA, USA
E-mail: rosenberg@oscillapower.com

Jennifer van Rij
National Renewable Energy Laboratory
Golden, CO, USA
E-mail: Jennifer.VanRij@nrel.gov

***Abstract*—The hydrodynamic forces acting on an oscillating multi-degree-of-freedom wave energy converter reaction body are characterized using scaled experiments and CFD simulations. Curves indicating how the hydrodynamic coefficients vary with Keulegan-Carpenter number (KC) and Reynolds number (Re) at four different scales, ranging from 1:75 to 1:36, are presented for multiple degrees of freedom. Understanding scale dependence is identified as important, as although representative KC numbers can be generated, the dissimilitude between the laboratory and full-scale Reynolds numbers requires careful consideration when inferring full-scale coefficients from the experiments. To address and examine this, CFD is used to replicate a number of these model-scale tests and provide simulations at full-scale. These results provide an important validation of some scaling trends but also reveal interesting discrepancies at low KC. We will show how these hydrodynamic relationships are replicated in different modes of motion, and illustrate their importance when building numerical models of WECs.**

***Index Terms*—heave plates/reaction bodies, hydrodynamics, CFD, point absorber, wave energy converter**

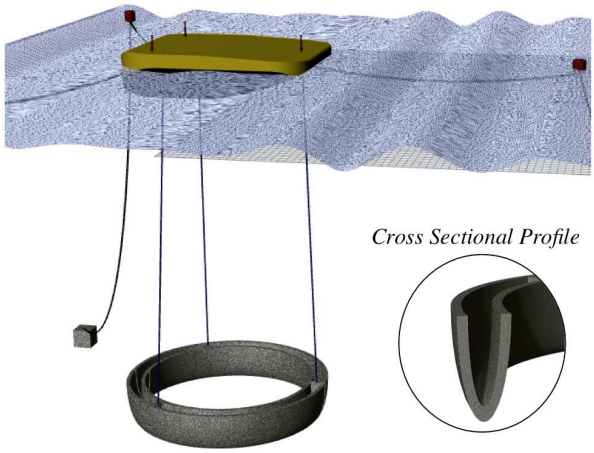

Fig. 1. TRITON™ WEC (*Oscilla Power, Inc.*). Inset shows reaction body cross-sectional profile (elliptical ogive).

I. Introduction

A. Background

Submerged 'heave plates' are commonly employed in point-absorbing wave energy converters (WECs) as a reaction body [1]–[3]. The hydrodynamic forces acting on this reaction body, in the form of added mass and drag, are important contributors to the overall reaction forces provided. These forces also have a significant influence on the overall WEC dynamics. The hydrodynamic added mass augments the structural mass and thus allows the reaction body to behave as if it is heavier, enabling greater reaction forces and increasing the natural resonance period(s) of the WEC [4], [5]. The drag contribution, which arises from separated flow vortices, turbulence and boundary layer friction, leads to viscous dissipation of energy and hence damping in the WEC system.

Some newer WEC's [6], [7] are using increasingly complex geometries for the submerged reaction body as a way of enhancing performance and survivability, especially in compliantly connected systems. An emerging challenge in creating mid-fidelity numerical models lies in accurately determining the hydrodynamic coefficients (added mass and drag) in the corresponding oscillatory flow regime for non-standard geometries [8]. While several simple canonical heave plate geometries, e.g. flat plates [9]–[11], have previously been characterized using forced oscillation experiments, there are limited studies that have focused on the coefficients generated by more complex geometries [7], [12]. Additionally, as most two-body WECs are heave-limited, little research has looked at reaction body hydrodynamics in additional degrees of freedom.

The recent emergence of some compliantly connected two-body WECs, such as the Oscilla Power (OPI) Triton (figure 1), requires consideration of the reaction body motions in multiple modes of motion (primarily heave & pitch, but also surge, sway, and roll) due to the multiple flexible tethers connecting the surface float to a ring-shaped reaction body. As such, it is necessary to characterize the full matrix of hydrodynamic coefficients in all relevant degrees of freedom.

The reaction body in this application is deployed at depth greater than 50m where wave excitation forces are small relative to the surface. For deep-water waves, the vertical fluid velocity reduces exponentially with depth such that approximately 96% of particle motion is attenuated at more than 1/2 wavelength below the surface [13]. This allows us to make the approximation that the surrounding fluid is quiescent.

As typical WECs can be several to 10's of meters in size, achieving a realistic Reynolds number in the laboratory is not practical. Therefore, when performing model-scale measurements, it is important to study and understand the impact of

limiting Reynolds number, and thus consider what value is high enough to enable similitude.

In this paper we present a series of experiments in which laboratory-scale Triton reaction bodies are sinusoidally forced to characterize the key hydrodynamic coefficients as functions of the two governing nondimensional parameters, Keulegan Carpenter number (KC) and Reynolds number (Re) [11], [14]. Experiments (regular sine waves) were performed over a range of representative KC and Re, where:

$$KC = \frac{2\pi \cdot z}{D} \tag{1}$$

and

$$Re = \frac{2\pi f \cdot z \cdot D}{\nu} \tag{2}$$

In equations 1-2, z is the oscillation amplitude, f is the oscillation frequency, D is a characteristic length scale and ν is the kinematic viscosity of water. As the reaction body studied here is an annulus, where the diameter is much larger than its width, the annulus width was selected as the relevant characteristic dimension.

Hydrodynamic characterizations of the key hydrodynamic properties (drag and added mass) are derived by fitting the experimental data to a Morison formulation [15], discussed in section III. Tank test results are compared against computational fluid dynamics (CFD) simulations in order to cross-validate both approaches and to allow parameters to be determined for much larger Re than can be achieved in the test tank. The CFD analysis also helps to provide some further insight into the flow regime.

B. Scaling & Objectives

As shown in equation 2, Re can be increased by either the oscillation frequency and/or the physical size. However, in order for representative experiments to be conducted in the laboratory, there are physical limitations on the dimensions of the test article. As previously mentioned, WECs often have large primary dimensions in the order of 10's of meters, and therefore there may be a substantial disconnect between what is possible at model scales and full-scale (1:1). The full scale reaction body for the Triton WEC is a 30m diameter ring, with a 3m characteristic dimension (annulus width). The objective of this work is therefore to understand how the hydrodynamic properties of reaction body's scale, allowing us to infer full scale values from small scale tests.

Froude scaling relationships are typically used for hydrodynamic tests that involve a strong interaction with surface waves and rely on Re independence, which is typically adequate if the Re is high enough and the flow is fully turbulent, but this work seeks to investigate this relationship further. However as seen in figure 2 as the scale reduces, the Re inequality can increase substantially. To investigate the limits of Re independence with respect to forced oscillation tests we examine four different test articles that are geometrically representative of the full scale article but reduced to scales

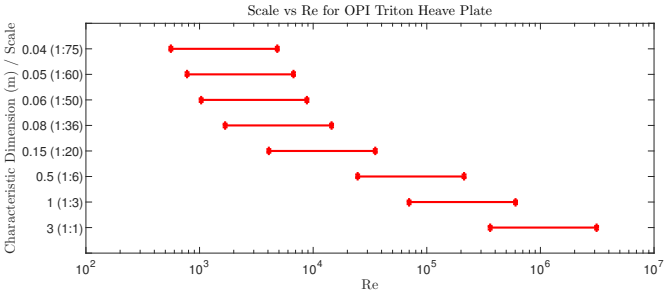

Fig. 2. Range of Re experienced with different scales if Froude or KC equivalence is enforced

1:75 1:60, 1:50 and 1:36. These scales are arbitrarily chosen, but their characteristic dimensions are typical of what might be achievable in a laboratory environment. Curves indicating how the hydrodynamic coefficients vary with (KC) and (Re) across these scales are presented for multiple degrees of freedom in section V.

The KC and Re values of the full-scale article are a function of the the environment that the WEC will operate in and the dynamics of the WEC itself. For this work, we selected the upper and lower 90th percentile of typical US west coast waves [16] as bounds for the wave conditions, then used a numerical simulation of the full-scale Triton WEC to identify equivalent KC and Re limits. These are shown in Table I.

TABLE I
90TH PERCENTILE Re AND KC LIMITS FOR THE OPI TRITON REACTION BODY IN A TYPICAL US WEST COAST WAVE CLIMATE.

	Lower Limit	**Upper Limit**
KC	0.31	7.85
Re	3.62×10^5	3.13×10^6

We were able to complete model tests for the aforementioned geometrically scaled models with KC values up to 6.28 and we also investigated the impact of a wide range of Re by oscillating each model over an order of magnitude in terms of frequency, from $0.5\ Hz$ to $5\ Hz$. In order to understand how the results from these models compared against 'full-scale' parameters, a detailed CFD analysis was also performed. In order to provide confidence in these numerical results, a number of the model scale tests were replicated directly before completing simulations at full-scale. These results provide an important validation of scaling trends and are presented and discussed in section IV.

II. Experimental Setup

A. Forced Oscillation Apparatus

To characterize the reaction ring hydrodynamic forces over a range of oscillation regimes, a plunging test apparatus was constructed, shown in figure 3. The test facility consists of a quiescent water basin (3.6 m in diameter, 1.15 m in depth) in which a geometrically scaled reaction ring is vertically oscillated using a pair of ball-screw linear actuators (providing

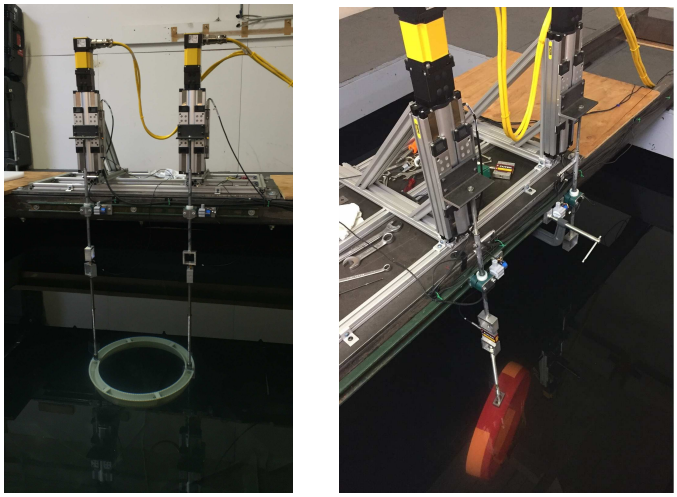

(a) Heave and pitch arrangement (b) Surge arrangement

Fig. 3. Images of the forced oscillation experiment

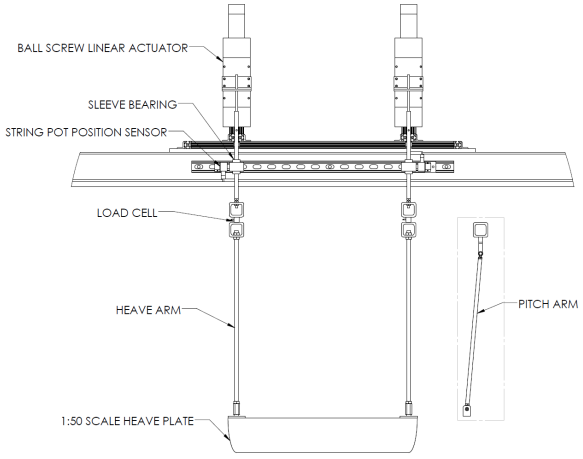

Fig. 4. Schematic of plunging apparatus. Waterline was just below the load cell bracket and the model was located mid water column. Tank is 3.6m in diameter with a water depth of 1.15m

up to $\sim$100 mm of travel and a maximum frequency of 5 Hz) each controlled by a servo motor and a feedback control system. A master displacement signal for both actuators is provided by an analog waveform generator built into the servomotor PID controller (Parker 6K-2), which was followed using encoder feedback from the motors.

The implementation of two actuators accommodates the annular shape of the body and allows the exploration of multi-modal response. Oscillating the two actuators in phase enables characterization of the translational drag and added mass (heave), while oscillating the actuators 180° out of phase enables characterization of the rotational drag and added moments of inertia (equivalent to pitch and roll). For measurements in surge, which is equivalent to sway, the reaction ring was rotated 90° and oscillated so that vertical motion in the experiment corresponds to its expected horizontal motion, as shown in figure 3(b). In this case, a single actuator was used.

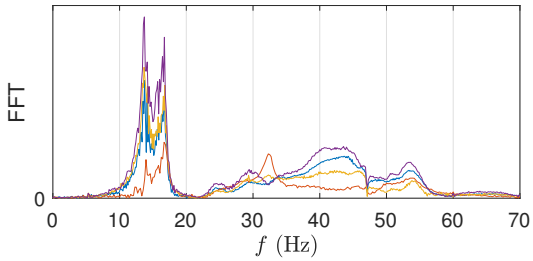

Fig. 5. Modal structural response of the gantry and plunging apparatus. Each curve represents the structure being excited at a different location.

Cylindrical support arms are connected between each actuator and at opposite sides of the annular reaction ring. Each support arm is supported by a sleeve bearing to prevent any lateral motion, underneath which load cells were installed between box section brackets. Different oscillation arms were used for heave and pitch. For heave measurements, rigid arms ($12mm$ steel) were threaded directly into an aluminum bracket fastened to the reaction ring. For pitch measurements, a clevis joint was used to enable pitch mobility but prevent roll motion, as shown in figure 4.

A direct measurement of the linear displacement of each actuator, relative to the stationary gantry, was made using an analog string potentiometer. The total force required to oscillate the reaction plate in water (which includes contributions from the hydrodynamic resistance force as well as the structural inertia of the rig components beneath the load cell) is measured using either a $10kg$ or $130kg$ S-beam load cell on each support arm. The displacement and force analogue signals were simultaneously acquired at 1 kHz using a National Instruments DAQ and Labview software.

The reaction rings were fabricated out of ABS in a consumer 3D printer using additive manufacturing (FDM) with a build volume of 317x203x254mm. This allowed the creation of identical representative models at multiple scales rapidly. For models larger than the printer, these were made by printing multiple (6-9) sections, which were then joined and bolted together. This process allowed models to be built and tested up to 1:36 scale, or approximately 1 m in diameter.

B. Experimental Considerations & Repeatability

Due to the inherent porosity associated with FDM, 3D printing is not always suitable for hydrodynamic models. As these models were fully submerged, there is a risk that the net mass may change during testing due to the release of entrapped air. In practice this did not pose a major issue and was mitigated by vigorously oscillating the reaction plate upon initial immersion to release any entrapped air. Additionally, the buoyancy force was monitored over the course of the tests and changes were observed to be negligible.

In order to mitigate free surface effects (above) and ground effects in the tank (below), the nominal reaction ring equilibrium position was vertically centered in the basin. Reasonable wait times were established between experiments to enable

the water to return to a quiescent state. To provide a gentle ramp-up to speed for each test, the actuators were first slowly translated to the extrema of travel, where the velocity in the cycle is zero. After waiting several seconds for any water disturbances to die down, the motion was initiated. During the tests, there was very little disturbance of the water surface, suggesting minimal free surface effects in the form of wave damping.

The vibrational resonances of the experimental arrangement were established by manually exciting (hitting) different parts of the plunging apparatus as well as the supporting gantry. FFT traces of the load cell signals are shown for multiple repetitions in figure 5, and demonstrate that there are no structural resonances around the oscillation frequencies of interest in the experiments. The dominant vibrational mode is approximately $15Hz$, which is well below the maximum oscillation frequency of $5Hz$.

In order to establish repeatability, multiple repeats of specific experiments were conducted to establish error margins. These were calculated to be in the oorder 9% for C_d and 3% for C_a.

III. Data Analysis

The Morison formulation [15] is a heuristic model that decomposes the net hydrodynamic force into an inertial term, which is in phase with acceleration, and a drag term that is proportional to the (square of the) velocity.

$$F = \rho C_a V \dot{u} + \frac{1}{2}\rho C_d A u\,|u| \tag{3}$$

The added mass coefficient C_a and drag coefficient C_d are then obtained through a fit to equation 3 using the measured hydrodynamic force F, velocity (u) and acceleration ($\dot{u}$). Here, the characteristic area A is taken to be the projected cross-sectional area in each DOF and the characteristic volume V is taken to be the displaced structural volume. Commonly, for flat plates, due to their minuscule displaced volume, V is typically taken to be an imaginary sphere about the plate, but due to the substantial wall thickness of the reaction body studied here, the physical displaced volume is appropriate as it leads to $\mathcal{O}(1)$ coefficients. A rotational analogue to the translational Morison formulation may be expressed as:

$$M = I_a \dot{\omega} + \frac{1}{2}\rho C_d A R^3 \omega\,|\omega| \tag{4}$$

Here, M is the net hydrodynamic moment, ω is the rotational velocity, R is the mean radius of the annulus, and I_a is the added moment of inertia (MoI), defined here as:

$$I_a = C_a\left(c\rho V R^2\right) \tag{5}$$

In the same way that the translational C_a can be interpreted as the ratio of the the added mass to displaced water mass, the rotational added mass coefficient, C_a, is defined here by normalizing the added MoI by the MoI of the displaced water, whereby c is a geometric constant associated with the reaction plate shape ($c = 0.5196$).

For each KC and Re tested, the reaction body was oscillated for 15 sinusoidal cycles. The load cell and displacement signals were low-pass filtered at 15 times the excitation frequency, and the velocity and acceleration of each actuator were inferred by differentiating the position signals. For all measurements, the displacement, velocity, and acceleration matched the prescribed value well, with correlation coefficients greater than 0.98. The load cells measure not only the hydrodynamic resistance force but also the inertial contribution due to the acceleration of the arms and reaction plate structural mass. This term was subtracted from the measured force signal to isolate the hydrodynamic force.

To calculate the hydrodynamic coefficients, a cycle averaging approach was used to create a single cycle ensemble of velocity, acceleration, and force. The first 5 cycles were discarded from the analysis to remove initial transients, and the final ten ensembles were then phase averaged and inserted into the Morison equation, where a least squares method was used to compute C_a and C_d.

In addition to these 'bulk' coefficient measurements, obtained through a full-cycle average, the forced oscillation tests were also used to assess how the vertical asymmetry of the reaction ring shape influences the hydrodynamics as it moves upward versus downward. Using the same cycle averaging approach, we first conditionally split the ensembles into two halves depending on whether the velocity was positive or negative before obtaining the coefficients from the Morison equation, using the same phase-averaged least-squares approach.

IV. Computational Model Setup

To validate the model-scale experimental results and trends for C_d and C_a, as well as estimate full-scale values, the CFD code STAR-CCM+ [17] is used. The hydrodynamic coefficients are evaluated in CFD in the same way as they are experimentally; specifically, C_d and C_a are calculated based on a simulated forced oscillation response. The forced oscillation response is modeled in STAR-CCM+ with the heave plate initially centered, both horizontally and vertically in the quiescent numerical water basin with applicable symmetries applied (x-z and y-z plane symmetries for heave, and x-z plane symmetry for pitch). For the model scale simulations the basin dimensions are identical to the physical basin, as illustrated in figure 6. For the full-scale simulations, the basin and ring dimensions are multiplied by 50. In STAR-CCM+, the forced oscillation response is realized by specifying the reaction ring velocity. As in the physical experiments, each simulation is run for $15T$, where T is the oscillation period, during which the ring position and resulting hydrodynamic forces and moments are recorded. Second-order temporal accuracy, with time-steps corresponding to a Courant number ($C = u\Delta t/\Delta x$) of 0.5, or less, are used for all simulations to assure numerical stability and accuracy.

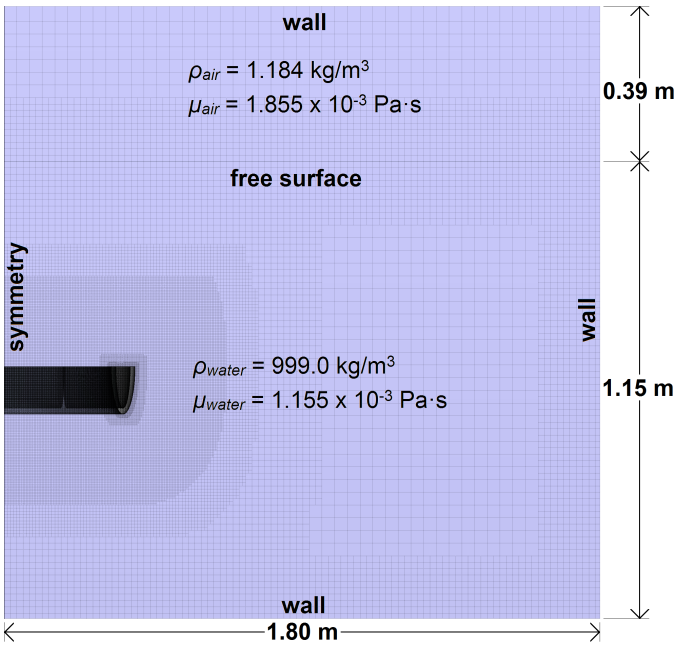

Fig. 6. Computational domain size, boundary conditions, grid resolution, and fluid properties for 1:50 scale forced heave oscillation CFD studies.

The CFD simulations are run with an implicit, unsteady, three-dimensional, Reynolds-averaged Navier-Stokes (RANS) model and the boundary conditions indicated in figure 6. For the turbulence closure model, the SST k-ω model, with 'all y^+ wall' treatment is utilized. The SST k-ω turbulence model is selected as it is a good compromise of computational stability, cost, and accuracy in capturing flow separation and recirculation. The all y^+ wall treatment is selected due to its broad applicability - for course mesh sizes, it tends towards a wall-function approach, while for low-Re, refined meshes, it tends towards the resolved viscous sublayer approach. The free surface is modeled using the Eulerian multiphase, volume of fluid (VOF) method, utilizing the fluid properties noted in figure 6.

To model the ring motion, a morphing mesh is utilized. The mesh, or grid, employed is illustrated in figure 6 for the 1:50 scale heave simulations. This grid was obtained via grid resolution and convergence studies. The grid refinement zones are based on minimizing the average y^+ on the heave plate and on the basin walls ($y^+_{avg,plate} \approx 2$ and $y^+_{avg,walls} \approx 7$ for the 1:50 scale simulations), as well as sufficiently resolving the velocity gradients surrounding the ring, while attempting to keep the total number of cells at a minimum. The resulting number of cells used for the heave and pitch simulations is 5.8×10^6 and 11.5×10^6, respectively. For the pitch simulations, the grid resolution and refinement zones are identical to the grid illustrated in figure 6, but without the y-z plane symmetry; and for the full-scale simulations, the grid is identical to the grid illustrated in figure 6, but proportionally enlarged by a factor 50.

V. Results

A. Experimental Measurements

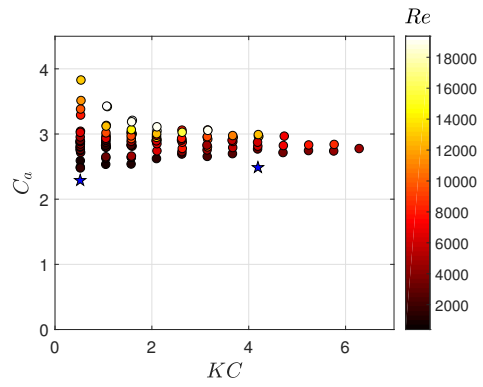

(a) Added mass coefficient (heave)

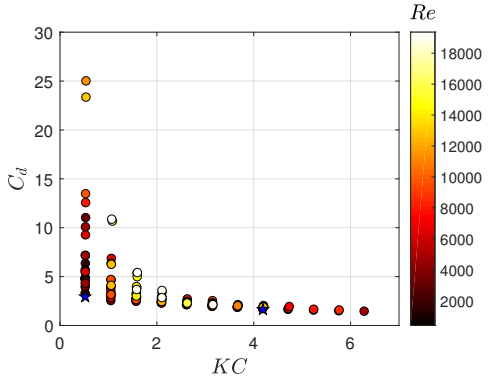

(b) Drag coefficient (heave)

Fig. 7. Experimental measurements for 1:75, 1:60, 1:50 & 1:36 scale geometries in heave. CFD data points at 1:50 scale (pentagrams) are shown for Tests H1 and H2, described in table II.

Experiments were conducted across a range of KC and Re with reaction rings of multiple scales as described above. The models were sinusoidally forced in heave, pitch and surge and the bulk hydrodynamic coefficients for drag and added mass are calculated as described and are presented in figures 7-9, for heave, pitch and surge, respectively. The data points represent the individual coefficients from all four scales tested, although for surge, due to the depth limitations of the basin, and the need to avoid free surface and bottom effects, only data at 1:75 scale is presented.

In heave, it can be seen the added mass coefficient, C_a, is loosely variant with Re (stronger variation for $KC < 2$), while for pitch and surge, it is largely invariant of Re. For all modes of motion C_a can be seen to be weakly nonlinear, exhibiting only a modest dependence on amplitude ($\sim$25% change over the order of magnitude in KC tested here). From the perspective of modeling this reaction body, this indicates that a linear added mass model, i.e. a constant C_a that is invariant with amplitude KC, is likely to capture the dynamics fairly well.

For all modes of motion, the drag coefficient C_d increases at low KC, which is consistent with previous studies of

oscillating structures [9], [14]. In heave, C_d has a strong Re dependency at low KC, which reduces as KC increases. In this low KC regime ($KC < 2$), C_d increases dramatically with Re. This is particularly interesting because previous studies on flat plates have shown that C_d is not very sensitive to Re and tends to slightly *decrease* with Re [11]. For each KC value tested, across different scales, the C_d tends to converge at high enough Re. As an example, C_d appears to converge at around 5 when $KC = 1.5$. As KC increases, the value of Re at which convergence occurs tends to reduce.

The full-scale (high Re) values for the drag coefficient might then be interpreted as lying on the trend formed by these asymptotic values. In surge, C_d displays the same Re dependent trend as in heave for $KC < 4$, although the range of surge Re numbers presented is not adequate to establish a fully converged C_d value, but should be explored further with experiments in a larger basin. Unlike for heave and surge, the pitch profile for C_d, shown in figure 8, displays little variation with Re and all the points appear to fall on roughly the same curve as a function of KC.

B. Numerical comparison to tank test results

Two sets of conditions were evaluated numerically. The low Re cases (H1, H2, P1, P2) were performed at 1:50 scale and

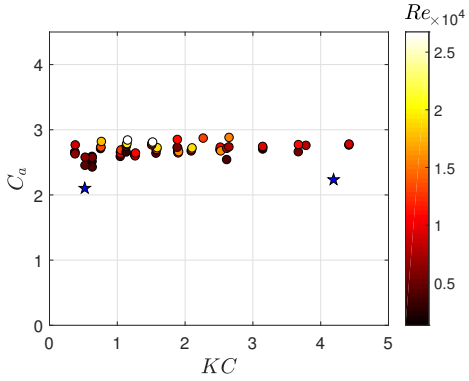

(a) Added MoI coefficient (pitch)

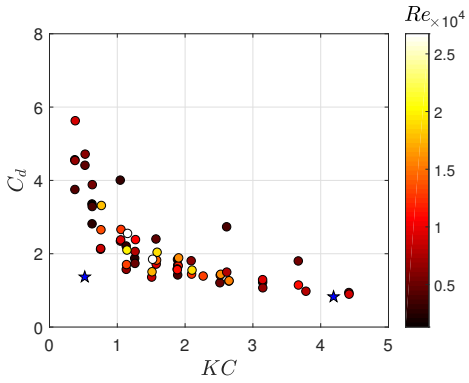

(b) Rotational drag coefficient (pitch)

Fig. 8. Experimental measurements for 1:75, 1:60, 1:50 & 1:36 scale geometries in pitch. CFD data points at 1:50 scale (pentagrams) are shown for Tests P1 and P2, described in table II.

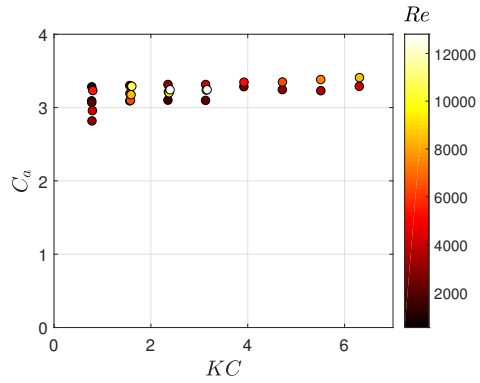

(a) Added mass coefficient (surge)

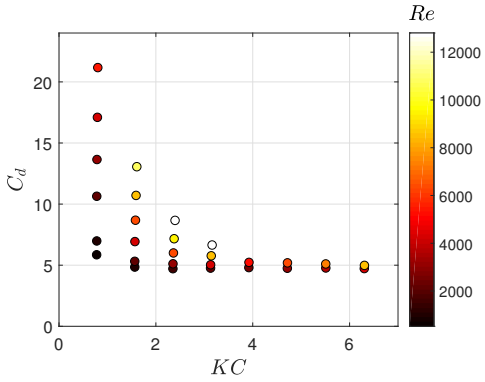

(b) Drag coefficient (surge)

Fig. 9. Experimental measurements for 1:75 scale geometries in surge.

were used as a comparison to the experimental runs. The high Re cases (H3, H4, P3, P4) were performed at full-scale and were used to generate coefficients for the full-scale Triton reaction body and to evaluate scaling trends predicted by the experiments for increasing Re. Table II shows the CFD test conditions in detail. The numerical conditions, for both the low and high Re cases, were selected to bookend the range of KC measured experimentally at 1:50 scale.

TABLE II
CFD TEST CASES

Test ID	DOF	Scale	z (m)	f (Hz)	KC	Re
H1	heave	1:50	0.005	1	0.52	1.63×10^3
H2	heave	1:50	0.955°	1	4.19	1.30×10^4
P1	pitch	1:50	0.04	1	0.52	1.63×10^3
P2	pitch	1:50	7.595°	1	4.15	1.29×10^4
H3	heave	1:1	0.25	$1/\sqrt{50}$	0.52	5.76×10^5
H4	heave	1:1	0.955°	$1/\sqrt{50}$	4.19	4.61×10^6
P3	pitch	1:1	2.0	$1/\sqrt{50}$	0.52	5.76×10^5
P4	pitch	1:1	7.595°	$1/\sqrt{50}$	4.15	4.57×10^6

The resulting C_d and C_a values are reported in table III for both a high grid resolution and a lower grid resolution. The

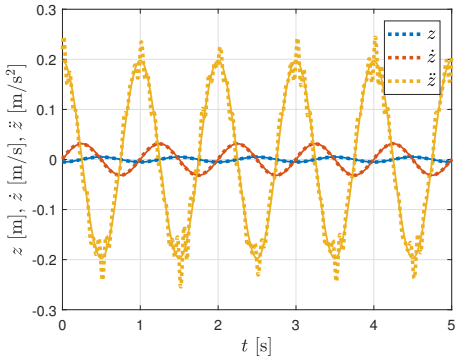

(a) Heave motion profiles. (—) CFD (- - -) Experiments.

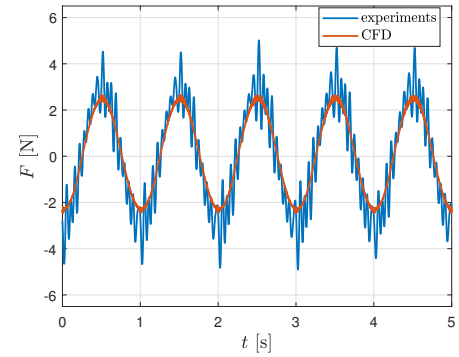

(b) Hydrodynamic force profiles in heave.

Fig. 10. Comparison between experiments and CFD for Test H1 (Low KC, 1:50 scale, heave).

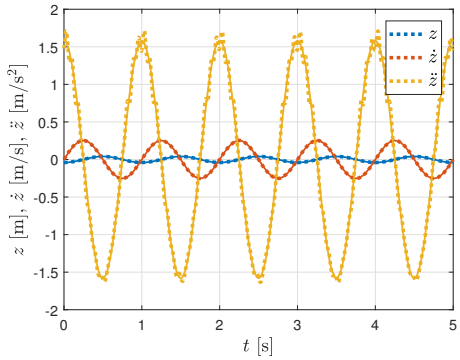

(a) Heave motion profiles. (—) CFD (- - -) Experiments.

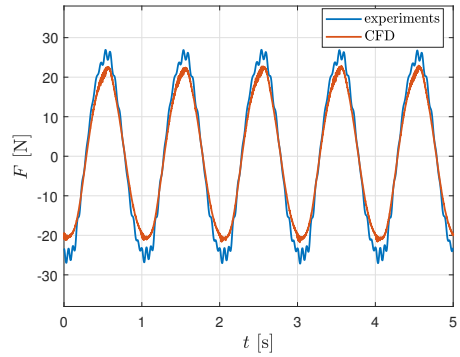

(b) Hydrodynamic force profiles in heave.

Fig. 11. Comparison between experiments and CFD. Test H2 (High KC, 1:50 scale, heave).

low grid resolution studies use the same grid topology, but with proportionally fewer cells; 0.8×10^6 and 1.6×10^6, for heave and pitch, respectively. On average, there is a 1.21% difference between C_a computed on the low and high grid resolutions, indicating excellent grid convergence. C_d computed using a high grid resolution are, on average, 9.75% lower than values computed using the low grid resolution; indicating a higher sensitivity to grid resolution, but still, reasonable convergence. Both free surface and ground effects are confirmed to be minimal for either grid resolution.

Time series motion and force comparisons to the tank experiments are shown in figures 10 and 11 for cases H1 and H2, respectively, which were conducted at matching scale, oscillation amplitude, and frequency. The force time history generally matches well with amplitude agreement to within 20%. The C_d and C_a values obtained from the 1:50 scale CFD are also plotted in figures 7-9 as a comparison against the experiments. Overall, there is fairly good agreement for added mass, C_a. With respect to drag, there is good agreement for C_d at high KC. At low KC the model-scale C_d matches fairly between experiments and CFD. However, a significant discrepancy was noted between experiments and CFD at low KC and high Re, where the experimental predictions at high Re are an order of magnitude above those from CFD. This is discussed further in section V-D.

TABLE III
CFD RESULTS FOR ADDED MASS AND DRAG COEFFICIENTS.

Test ID	C_a (Low Grid Resolution)	C_d (Low Grid Resolution)	C_a (High Grid Resolution)	C_d (High Grid Resolution)
H1	2.234	3.165	2.288	2.937
H2	2.512	1.689	2.486	1.633
P1	2.069	1.496	2.102	1.367
P2	2.258	0.849	2.234	0.827
H3	2.222	2.686	2.232	2.179
H4	2.511	1.643	2.467	1.538
P3	2.054	1.174	2.058	0.983
P4	2.247	0.811	2.220	0.769

C. Asymmetry of coefficients

As shown in figures 10 and 11, the hydrodynamic force is fairly symmetrical with respect to direction of motion for these two test cases. To explore the effect of geometric asymmetry more closely, the conditional averaging approach, discussed in section III, was used to extract directional coefficients. The ratio of the 'upwards' and 'downwards' coefficients for the tank tests is presented in figure 12.

For $KC > 2$, asymmetry in drag is small, with a variation of less than 20% between the 'upwards' versus 'downwards' coefficients for this geometry. Similarly, there does not appear

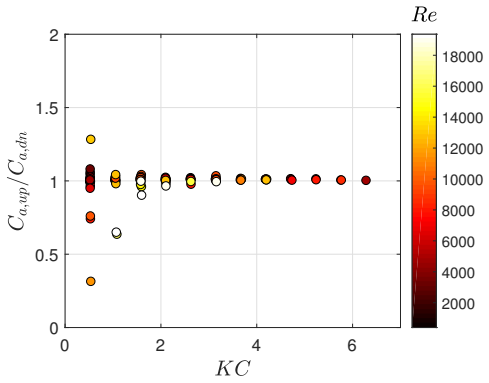

(a) Added mass coefficient (heave)

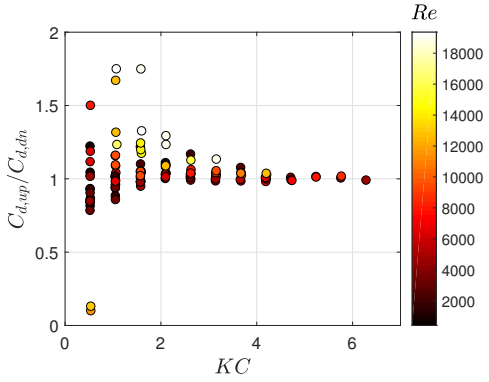

(b) Drag coefficient (heave)

Fig. 12. Experimental measurements in heave demonstrating the asymmetry of the coefficients.

to be any significant directional variability in added mass, which is perhaps to be expected, due to the symmetry of 'pushing' versus 'pulling' surrounding water mass. At low KC, however, there is significant apparent asymmetry in the both the drag and added mass, which will be investigated in future studies, and might be related to the discussion in section V-D.

D. Discrepancy between CFD results and Tank tests

The following have been identified as possible reasons for the discrepancy between the CFD and experiments at low KC and high Re:

Measurement Sensitivity: It is important to appreciate that KC can be interpreted as the ratio of drag to inertia force, which means that the drag force component is smaller at low KC. In figures 10-11, even at high KC, it is evident that the added mass force dominates compared to the drag force since the measured force is in phase with acceleration and is small at maximum velocity. This is significant because it means that measuring C_d accurately will be challenging since the drag force is a relatively small component of the overall hydrodynamic force and is perhaps quite sensitive to measurement accuracy and/or methodology. To further demonstrate this point, figure 13 shows the reconstructed force profiles for Test H1, obtained from the Morison equation using

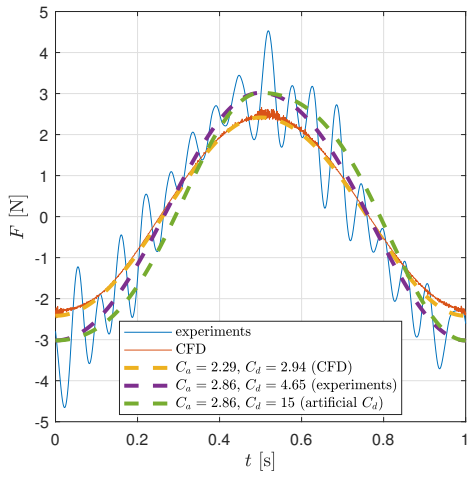

Fig. 13. Reconstructed fit of CFD and experimental data to the Morison equation. Dashed lines are produced from the best-fit coefficients. Note the only slight difference when C_d is increased by a factor of three, illustrating the dominance of added mass in this condition (Test H1).

the best-fit coefficients from the tank tests and CFD. Even artificially increasing C_d by a factor of three results in little noticeable change in the force profile, illustrating the very small contribution from drag.

Numerical Representation of Turbulence: The CFD results presented relied upon a RANS approach. Additional CFD investigation may be useful to identify if resolving turbulence more accurately leads to a different result, for example, using a large eddy simulation (LES).

Different Oscillation Regimes: Re can be increased either by increasing the reaction plate size or by increasing the oscillation frequency. While a smaller size and higher frequency can produce the same Re as a slower and larger structure, the underlying physics and flow regimes may be different due to the vertical extent of the reaction body. The very large C_d values that we see experimentally (10-25) are from high frequency tests. Figure 14 presents a series of figures showing how, experimentally, at 1:50 scale with constant amplitude KC, the structure of the force signal changes as f increased, which is especially clear at $5Hz$. Although the shape of the measured hydrodynamic force modulates with increasing f, the forces shown in the full-scale CFD simulation remains sinusoidal. This might imply a different operating regime and we speculate that another nondimensional parameter may be involved in the problem since a new length scale has been introduced (the vertical height of the structure). Limited studies have focused on 3D structures [12] and typically 2D structures of small thickness predominate in the literature. If KC is small, then the structure is oscillating within its length, and thus at high frequency, the plate might turn back into its own wake before previous vortices have time to advect away. However, at lower velocities and larger dimensions, the wake may have chance to stabilize between oscillations. We postulate that the ratio of the vertical structure extent to the

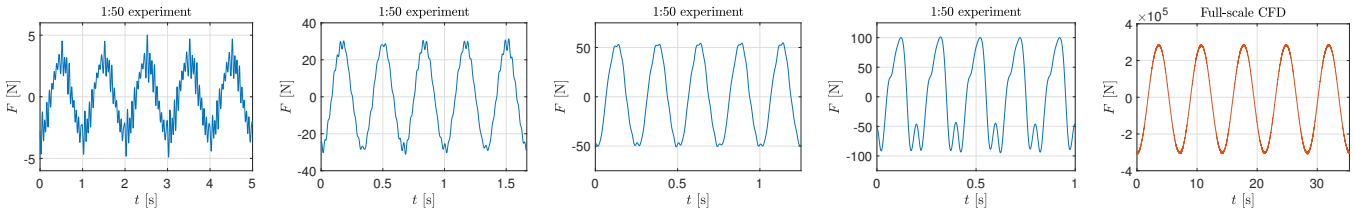

(a) $f = 1$ Hz, $Re = 1.6 \times 10^3$(b) $f = 3$ Hz, $Re = 4.7 \times 10^3$(c) $f = 4$ Hz, $Re = 6.3 \times 10^3$(d) $f = 5$ Hz, $Re = 7.9 \times 10^3$ (e) $Re = 5.8 \times 10^5$

Fig. 14. The force profiles shown are all at identical $KC = 0.52$. Plots show how increasing Re by increasing f at 1:50 scale appears to change the structure of the flow, as evidenced by the force signals. This is compared to a full-scale CFD simulation (i.e. high Re), which demonstrates a different, more sinusoidal, structure.

characteristic length may provide an additional nondimentional number, and that at some value, the Re invariance seen at higher KC may not apply. Such a parameter would be used to define a limit to the validity of scale assumptions for these types of tests.

VI. Conclusion

1) In general, hydrodynamic coefficients tend to asymptote to a fixed value for a given KC as Re increases. however,
2) At higher KC values the added mass coefficients agree fairly well between CFD and model tests. Scaling trends are illustrated and appear to confirm Re invariance above a certain threshold.
3) A significant disconnect was observed between CFD measurements and tank test predictions at low KC numbers when using high Re values. While the authors accept that this could be due to inaccuracy in either the CFD model or the experimental measurement, the order of magnitude of the discrepancy suggest that this may be unlikely. If we assume the CFD data point is real, this implies that there may be a limit to the minimum physical scale required to allow similitude in low KC experiments.
4) Typically similitude between a large scale item moving slowly can be generated by a smaller model scale item moving fast. At high KC, this appears to generate the same hydrodynamic coefficients as long as Re is above a certain threshold. At low KC however the trends in the hydrodynamic experiments suggest that for smaller scales, a substantial overestimation in the coefficients will be achieved even if Re equivalence is achieved. Work is needed to confirm what the scale limit is before equivalence is achieved, but it is postulated that it may be a function of the ratio of the structure vertical extent to its the characteristic dimension.

VII. Further Work

The overarching goal of this research is to produce a fairly accurate low-order dynamical model for the Triton reaction body, which can then be implemented in a mid-fidelity model of the full WEC. The data demonstrate that in certain regimes, the hydrodynamic coefficients, particularly for drag, can be fairly nonlinear and exhibit amplitude (KC) dependence. Incorporating this behavior in a time-domain model, by varying the coefficients dynamically with the local KC, will be explored and evaluated for accuracy against full-WEC wave basin test results. Capturing this behavior is particularly important in real irregular seas, where KC varies each cycle. Although this work was limited to regular waves, a knowledge of how these hydrodynamic coefficients will vary in irregular waves is needed to improve the quality of mid-fidelity models. Further work will look at using irregular forced oscillations (e.g. white noise or JONSWAP spectra) in conjunction with system identification techniques [18] to compare with the regular wave tests and capture potential nonlinear or coupling effects between the oscillation modes.

Additional work is planned to further examine the high Re discrepancy between tank and numerical results at low KC.Visualizing the flow patterns about the experimental models, using bubble or dye injection, may help illustrate the mechanisms behind the large increase in C_d at high oscillation frequency. It is hoped that further RANS CFD analysis, or potentially LES, can be used to study the flow behavior in this regime. We also aim to further investigate the hypothesis of the existence of an additional non-dimensional parameter that becomes relevante for 3D structures of large vertical extent.

Acknowledgment

OPI gratefully acknowledges support from the U.S. Department of Energy (through award no. DE-EE0007346) as well as Andrew Gill for his assistance with the experiments.

References

[1] www.oceanpowertechnologies.com.
[2] http://columbiapwr.com/.
[3] V. S. Neary, M. Previsic, R. A. Jepsen, M. J. Lawson, Y. Yu, A. E. Copping, A. A. Fontaine, K. C. Hallett, and D. K. Murray, "Methodology for design and economic analysis of marine energy conversion (MEC) technologies," *Sandia Technical Report*, no. 2014-9040, March 2014.
[4] J. C. C. Henriques, M. F. P. Lopes, R. P. F. Gomes, L. M. C. Gato, and A. F. O. Falcao, "On the annual wave energy absorption by two-body heaving wecs with latching control," *Renewable Energy*, vol. 45, pp. 31–40, 2012.
[5] C. Liang and L. Zuo, "On the dynamics and design of a two-body wave energy converter," *Renewable Energy*, vol. 101, pp. 265–274, 2017.
[6] B. J. Rosenberg and T. R. Mundon, "Numerical and physical modeling of a flexibly-connected two-body wave energy converter," in *4th Marine Energy Technology Symposium*, Washington, D.C., 2016.

[7] A. C. Brown and J. Thomson, "Phase-resolved heave plate dynamics for wave energy converters," in *4th Marine Energy Technology Symposium*, Washington, D.C., 2016.
[8] T. R. Mundon, "Progress in the hydrodynamic design of heave plates for wave energy converters," in *International Conference on Ocean Energy*, Edinburgh, Scotland, 2016.
[9] J. Li, S. Liu, M. Zhao, and B. Teng, "Experimental investigation of the hydrodynamic characteristics of heave plates using forced oscillation," *Ocean Engineering*, vol. 66, pp. 82–91, 2013.
[10] L. Tao and D. Dray, "Hydrodynamic performance of solid and porous heave plates," *Ocean Engineering*, vol. 35, no. 10, pp. 1006–1014, 2008.
[11] C. C. Shih and H. J. Buchanan, "The drag on oscillating flat plates in liquids at low Reynolds numbers," *Journal of Fluid Mechanics*, vol. 48, no. 02, pp. 229–239, 1971.
[12] C. J. Rusch, B. Maurer, T. R. Mundon, A. Stewart, and B. Polagye, "Hydrodynamics and scaling of heave plates for point absorbing wave energy converters," in *European Wave and Tidal Energy Conference*, Cork, Ireland, September 2017.
[13] B. Cushman-Roisin, *Environment Fluid Mechanics*. USA: John Wiley and Sons, Inc., 2014.
[14] G. H. Keulegan and L. H. Carpenter, "Forces on cylinders and plates in an oscillating fluid," *J. Res. Nat. Bur. Stand.*, vol. 60, no. 5, May 1958.
[15] J. Morison, J. Johnson, S. Schaaf *et al.*, "The force exerted by surface waves on piles," *Journal of Petroleum Technology*, vol. 2, no. 05, pp. 149–154, 1950.
[16] A. R. Dallman and V. S. Neary, "Characterization of us wave energy converter (wec) test sites: A catalogue of met-ocean data." Sandia National Laboratories (SNL-NM), Albuquerque, NM (United States), Tech. Rep., 2014.
[17] *"STAR-CCM+" [Online]. Available: http://mdx.plm.automation.siemens.com/star-ccm-plus. [Accessed: 02-Mar-2017].*
[18] G. Bacelli, R. G. Coe, D. Patterson, and D. Wilson, "System identification of a heaving point absorber: Design of experiment and device modeling," *Energies*, vol. 10, no. 4, p. 472, 2017.